factors $\leq 7\times 10^4$ are known. The 15.9-keV transition is K-forbidden: $\nu=\Delta K-3=2$. For each unit of ν a retardation factor between 10 and 100 is found to be the rule, in agreement with the present result. No special search for the 13.5-keV transition from the 169-keV to the 156-keV level was undertaken as this transition is equally K-forbidden as the 106-keV transition ($\nu=1$) with which it competes: It is therefore expected to be $(106/13.5)^3\sim 500$ times weaker. The absence of the 156-keV ($<0.1\%$) and 169-keV ($<0.05\%$) $E2$ transitions is attributed to the preferred role of the competing 92- and 106-keV $M1$ transitions.

ACKNOWLEDGMENTS

We wish to thank J. A. Baranosky for the separation of Tc^{199m} from fission fragments, Dr. Elizabeth Baker for help and advice concerning the electroplating of Re films, and T. W. Moffett for his preparation of evaporated Re films. We are indebted to Dr. John Mihelich for his encouragement at the beginning of this experiment.

PHYSICAL REVIEW VOLUME 136, NUMBER 1B 12 OCTOBER 1964

Spin and Magnetic Moment of N^{13}†

A. M. Bernstein,* R. A. Haberstroh,‡ D. R. Hamilton, M. Posner,§ and J. L. Snider**
Palmer Physical Laboratory, Princeton University, Princeton, New Jersey
(Received 13 April 1964)

The spin and hyperfine structure separation $\Delta\nu$, of 10-min N^{13} have been measured by the atomic-beam magnetic-resonance technique. The atomic-beam machine was a modified focusing apparatus consisting of a six-pole A magnet, a Goodman-type C magnet, and an approximately uniform-gradient B magnet. This apparatus, which combines the high transmission of focusing machines and the smaller detector area of conventional machines, is described in detail. The N^{13}, in the form of a gaseous molecule, was flushed continuously from the cyclotron target to the apparatus, where neutral atoms were produced in a microwave discharge in the neon carrier gas. The beam was detected on titanium foils heated to approximately 1025°C. The measurements were made in the $^4S_{3/2}$ atomic ground state, but resonances were also observed in the ^2P and ^2D metastable doublets. The final results are $I=\frac{1}{2}$, as expected, and $\Delta\nu=33.347\pm 0.020$ Mc/sec from a $\Delta F=1$ measurement. Using the high-precision results on N^{14} and N^{15}, we obtain an average value of $|\mu_I|$, which, corrected for shielding, is $|\mu_I|=0.32212\ (36)$ nm. Assuming that the sign is negative (as in the case of N^{15}), the sum of the magnetic moments of N^{13} and C^{13} is 0.380 nm, in agreement with the combined predictions of Kurath (for the ordinary part of the magnetic moment operator) and Sachs (for the mesonic current contributions). Further discussion of the result is given.

I. INTRODUCTION

THE study of nuclear magnetic dipole moments has an extensive literature.[1] Experimentally one can make measurements with great precision, but theoretically the situation is not so clear.

The calculation of magnetic moments is very sensitive to small configuration admixtures in the nuclear wave functions.[2] If this were the only uncertainty, then one could use the measured quantities to deduce information about these wave functions. However, it has been shown that the form of the nuclear magnetic dipole operator is sensitive to the strong interactions of the nucleons,[3] i.e., sensitive to meson exchange currents. This differs from the case of electric multipole operators for which the form of the electromagnetic interaction should be independent of the other interactions of the nucleons.[3]

In addition, there has long been speculation about using the same g factors for bound nucleons as for free nucleons.[4] There are large contributions to the nucleon g factors from virtual emission and absorption of mesons, which involve the recoil of the nucleon. In finite nuclei, recoils into occupied momentum states are prohibited by the Pauli principle which could result in a quenching of the g factor. A recent calculation has shown this to be an appreciable effect.[5]

It was pointed out[6] that the meson exchange contribution to a pair of mirror nuclei should be equal and

† This work was supported in part by the U. S. Atomic Energy Commission and the Higgins Scientific Trust Fund.
* Present address: Massachusetts Institute of Technology, Cambridge, Massachusetts.
‡ Present address: Heidelberg University, Heidelberg, Germany.
§ Present address: Yale University, New Haven, Connecticut.
** Present address: Harvard University, Cambridge, Massachusetts.

[1] For a general review of the subject see R. J. Blin-Stoyle, Rev. Mod. Phys. 28, 75 (1956).
[2] H. Noya, A. Arima, and H. Horie, Progr. Theoret. Phys. (Kyoto) Suppl. 8, 33 (1958) and R. J. Blin-Stoyle, Proc. Phys. Soc. (London) A66, 1158 (1953).
[3] R. G. Sachs, *Nuclear Theory* (Addison-Wesley Publishing Company, Cambridge, Massachusetts, 1953), Chap. 9.
[4] F. Bloch, Phys. Rev. 83, 839 (1951), A. de Shalit, Helv. Phys. Acta 24, 296 (1951), and H. Miyazawa, Progr. Theoret. Phys. (Kyoto) 6, 801 (1951).
[5] S. D. Drell and J. D. Walecka, Phys. Rev. 120, 1069 (1960).
[6] For references to the original literature see Refs. 1 and 3.

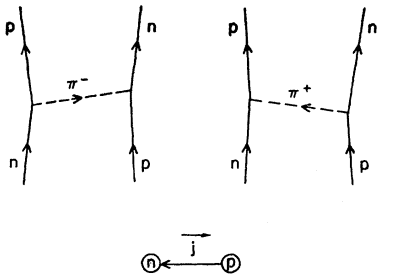

FIG. 1. Feynman diagrams for meson exchange currents.

opposite. One can see this physically as follows. Consider an interaction in which a neutron changes into a proton by either emitting a π^- meson or absorbing a π^+ meson (Fig. 1). In either case, the current vectors go from proton to neutron. The mirror transformation sends all neutrons into protons and vice versa. As a result, all of the exchange current vectors are reversed in the mirror nucleus, and therefore the sum of the magnetic moments of a pair of mirror nuclei should be independent of mesonic exchange effects. In the charge symmetric approximation mirror nuclei have identical space spin-wave functions (e.g., Ref. 3), and information about the wave functions can be obtained from the sum of the moments. In the case of He^3 and H^3, by assuming that the wave function is $\psi=\alpha\,{}^2S_{1/2}+\beta\,{}^4D_{1/2}$, Sachs[3] determined from the sum of the experimental moments that $\beta^2=0.04$ and then, by comparing the experimental moments with the ones calculated (Table I) with the wave function given above, found that there is a discrepancy of 0.27 nm, which he ascribed to meson exchange currents.

At the time that the present experiment was begun, He^3 and H^3 were the only mirror pair (besides the neutron and proton) for which both magnetic moments were known. N^{13} was chosen because it could be made in the Princeton cyclotron in a gaseous molecule which could be flushed continuously out of the cyclotron target into the atomic-beam machine. In addition, its relatively long half-life (10 min) simplified many experimental problems.

II. RELEVANT RESULTS FROM HYPERFINE STRUCTURE THEORY

The theory of hyperfine structure has been fully described elsewhere.[7] Only a brief summary of the results pertinent to this experiment will be given here.

TABLE I. Summary of the He^3-H^3 magnetic moment anomaly. μ_{exp} is the experimental moment and μ_{th} is the theoretical moment calculated by Sachs[a] for a wave function of 96% ${}^2S_{1/2}$ and 4% ${}^4D_{1/2}$.

	μ_{exp}	μ_{th}	$(\mu_{exp}-\mu_{th})$
He^3	−2.127	−1.86	−0.27
H^3	2.979	2.71	0.27

[a] See Ref. 3, Chap. 9.

[7] For a general review of atomic beams, theory and techniques, see N. F. Ramsey, *Molecular Beams* (Oxford University Press, Oxford, England, 1956), and P. Kusch and V. W. Hughes, *Handbuch der Physik*, edited by S. Flügge (Springer-Verlag, Berlin, 1957), Vol. 37, pp. 1–172.

Nitrogen has a ${}^4S_{3/2}$ ground atomic state, with $g_J=2.002114(4)$.[8] N^{13} was expected to have nuclear spin $I=\frac{1}{2}$ because this is the known spin of C^{13}. For such a case, when either I or J is $\frac{1}{2}$, quadrupole and higher order interactions are not effective, and the effective hyperfine Hamiltonian takes the simple form

$$\mathcal{H}=ha(\mathbf{I}\cdot\mathbf{J})+g_J\mu_0(\mathbf{J}\cdot\mathbf{H}_0)+g_I\mu_0(\mathbf{I}\cdot\mathbf{H}_0)\,, \qquad (1)$$

where a is the magnetic dipole hyperfine interaction constant; μ_0 is the Bohr magneton, $\mathbf{H}_0$ is the external magnetic field, g_I and g_J are the atomic and nuclear g factors, and the sign convention for the g factors follows that of Refs. 7; $g_I=-\mu_I/\mu_0 I$ and $g_J=-\mu_J/\mu_0 J$. In zero magnetic field the atomic state is split into a number of degenerate levels specified by the total angular momentum $\mathbf{F}=\mathbf{I}+\mathbf{J}$, with values given by the usual vector rule, in this case $F=2$ and $F=1$. Application of a weak magnetic field results in a further splitting of each F level into $(2F+1)$ equally spaced sublevels labeled by values of m_F, the projection of $\mathbf{F}$ in the magnetic-field direction. The transition frequency for low-field Zeeman transitions satisfying the selection rules $\Delta F=0$, $\Delta m_F=\pm 1$, is

$$\nu_{\text{Zeeman}}=g_F\mu_0 H_0/h\,,$$

where

$$g_F\cong\{[F(F+1)+J(J+1)-I(I+1)]/2F(F+1)\}g_J\,.$$

A term in g_I has been neglected in this expression, since $g_I\ll g_J$.

Verification of $I=\frac{1}{2}$ therefore consists in the observation at several different field strengths of weak-field transitions at the frequencies predicted by the above relations using the known values of J and g_J and assuming $I=\frac{1}{2}$, and at no other frequencies. In this experiment Ar^{40} was used to calibrate the magnetic field. The transition frequency for $Ar^{40}(I=0)$ in its ${}^3P_2$ metastable state is

$$\nu(Ar^{40})=g_J\mu_0 H_0/h\cong\tfrac{3}{2}(\mu_0 H_0/h)\,.$$

In this way the nuclear spin was confirmed to be $\frac{1}{2}$, as described more fully below.

At stronger magnetic fields the N^{13} transition frequencies no longer vary linearly with field. When $I=\frac{1}{2}$, the dependence of energy on field is given analytically by the Breit-Rabi formula, which for $I=\frac{1}{2}$, $J=\frac{3}{2}$, and $a<0$ takes the form

$$E(F,m_F)/h\Delta\nu=\tfrac{1}{8}+(g_J\mu_0 H_0/h\Delta\nu)m_F \mp\tfrac{1}{2}(1+Xm_F+X^2)^{1/2}, \qquad (2)$$

where

$$\Delta\nu=2|a| \quad\text{and}\quad X=(g_J-g_I)\mu_0 H_0/h\Delta\nu\,.$$

[8] M. A. Heald and R. Beringer, Phys. Rev. **96**, 645 (1954).

The minus sign holds for $F=2$, the plus sign for $F=1$. For the ($F=2$, $m_F=1$) to ($F=2$, $m_F=0$) transition the frequency is

$$\nu_{[(2,1)\to(2,0)]}/\Delta\nu=(g_J\mu_0H_0/h\Delta\nu) -\tfrac{1}{2}(1+X+X^2)^{1/2}+\tfrac{1}{2}(1+X^2)^{1/2}. \quad (3)$$

This was the transition used to obtain preliminary values of $\Delta\nu$ at successively higher magnetic fields until an observation could be made of the direct transition between ($F=1$, $m_F=0$) and ($F=2$, $m_F=0$) (in very weak fields). The frequency of this transition is

$$\nu_{[(1,0)\to(2,0)]}/\Delta\nu=(1+X^2)^{1/2}. \quad (4)$$

In this case, two $\Delta F=1$, $\Delta m_F=0$ transitions in K^{39} were used to calibrate the field. Their frequencies differed from $\Delta\nu(K^{39})$ by $\pm 2\nu_Z(K^{39})$, where the K^{39} Zeeman frequency, $\nu_Z(K^{39})$, is given by

$$\nu_Z(K^{39})=g_F\mu_0H_0/h\cong\tfrac{1}{2}(\mu_0H_0/h). \quad (5)$$

In terms of $\nu_Z(K^{39})$, we get the final result, sufficiently good for our purposes:

$$\Delta\nu=\nu_{[(1,0)\to(2,0)]}\times\left[1-8\left(\frac{\nu_Z(K^{39})}{\Delta\nu}\right)^2\right]. \quad (6)$$

Figure 2 shows the hyperfine energy levels of N^{13} as a function of magnetic field assuming $a<0$. The particular $\Delta F=0$ transition used in the preliminary measurements of $|a|$ is indicated, as well as the $\Delta F=1$ transition used in the final measurement. The evaluation of the magnetic moment itself from a will be described in the discussion of the experimental results.

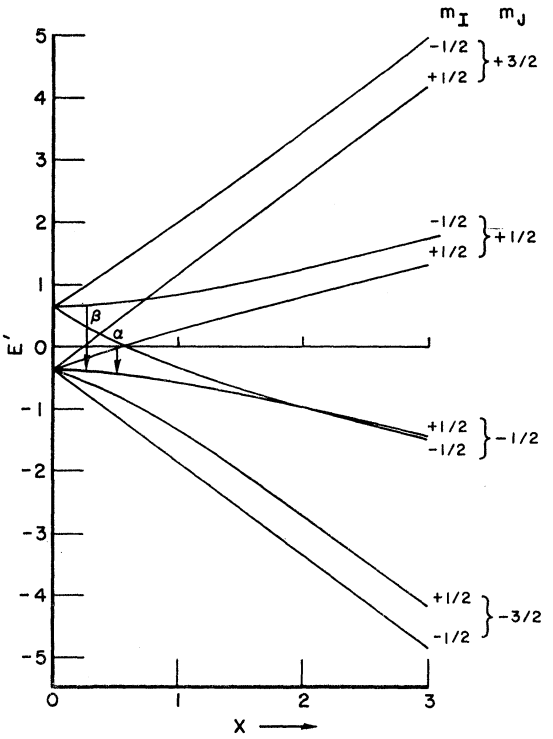

FIG. 2. Energy level diagram of the hyperfine structure of N^{13} in the $^4S_{3/2}$ ground atomic state as a function of the magnetic field, H_0 (for $I=\frac{1}{2}$ and assuming $a<0$). The observed transitions in the $\Delta F=0$ and $\Delta F=1$ work are denoted by α and β, respectively. $E'=E/h\Delta\nu$ and $x=(g_J-g_I)\mu_0H_0/h\Delta\nu$ ($g_I/g_J\ll 1$ used).

III. ATOMIC-BEAM APPARATUS

A. General Principles

The atomic-beam magnetic-resonance apparatus was designed to be a "flop-in" apparatus which would preserve the increased beam intensity at the detector achieved by the use of focusing magnets[9] and which would, at the same time, possess the small detector area and consequent high signal-to-background ratio characteristic of a nonfocusing apparatus.

In previously constructed focusing machines[9–11] both the A and B magnets are focusing (six-pole). In a six-pole B magnet the flopped beam diverges from the magnet axis, making a detector of considerable area necessary. As both the machine and counter backgrounds increase with detector area, a decrease in the detector area without a sacrifice in intensity was considered desirable. It was observed that the focusing property of the six-pole machines was obtained from the A magnet; the function of the B magnet is to separate and transmit the flopped and the unflopped atoms. It is possible to use for this purpose a two-pole, constant gradient, B magnet without seriously decreasing the focused beam intensity. This procedure has the advantage that the beam size is unaffected by the B magnet; a much smaller detector can therefore be used with a corresponding decrease in the machine and counter backgrounds.

In a strong, inhomogeneous magnetic field in which **I** and **J** are decoupled, the force on an atom is

$$\mathbf{F}\cong -g_Jm_J\mu_0\nabla|\mathbf{H}|,$$

where $\nabla|\mathbf{H}|$ is the gradient of the magnitude of the magnetic field $\mathbf{H}$(g_J, as defined in Sec. II, is normally positive). Choosing x to be the transverse deflection of an atom (assumed small) in a gradient $\nabla|\mathbf{H}|$ (assumed transverse) and $z=vt$ to be the longitudinal coordinate in the beam direction, the equation of motion takes the form

$$\frac{d^2x}{dz^2}=\left(\frac{1}{v^2}\right)\frac{d^2x}{dt^2}=-\frac{g_Jm_J\mu_0\nabla|\mathbf{H}|}{mv^2}=-\gamma\nabla|\mathbf{H}|. \quad (7)$$

The orbit of an atom in a transverse deflecting field is thus completely determined by the value of the parame-

[9] A. Lemonick, F. H. Pipkin, and D. R. Hamilton, Rev. Sci. Instr. 26, 1112 (1955).
[10] I. Lindgren, Nucl. Instr. 3, 1 (1958).
[11] H. M. Goldenberg, D. Kleppner, and N. F. Ramsey, Phys. Rev. 123, 530 (1961).

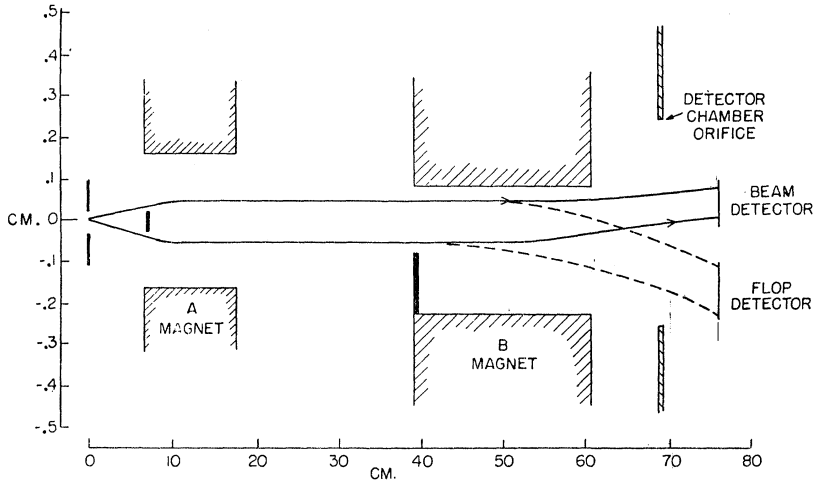

FIG. 3. Schematic orbits in the apparatus (top view). Note the expanded vertical scale. The A and B magnet stops are shown as heavy black lines.

ter γ, defined as

$$\gamma = g_J m_J \mu_0 / mv^2.$$

For a six-pole magnet the gradient is radial and given by $\nabla|\mathbf{H}| = \alpha \mathbf{r}$, where $\mathbf{r}$ is the radius vector measured from the magnet symmetry axis. For a two-pole magnet shaped to produce a quadrant of a four-pole field for which $|\mathbf{H}| \propto r$, $\nabla|\mathbf{H}|$ is approximately constant over the beam (see following section, B.2.b). Atomic orbits through a system of a six-pole followed by a two-pole magnet are shown schematically in Fig. 3. The function of each magnet is the following: (1) The A magnet serves to focus and polarize the beam. Atoms with $m_J > 0$ (for positive g_J) have $\gamma > 0$ and are transmitted, being attracted towards the axial weak-field region or focused; atoms with $m_J < 0$ have $\gamma < 0$ and are not transmitted, being deflected away from the axis into the magnet pole pieces; (2) the B magnet separates the atoms which have undergone resonance transitions in which m_J changes sign (i.e., atoms which are "flopped") from the atoms which still have $m_J > 0$ (i.e., the "unflopped" beam). Atoms with $m_J < 0$ are deflected towards the strong-field pole tip and detected at the flop detector as a resonance signal. Ideally, the beam intensity at the flop detector is zero in the absence of a resonance.

B. Detailed Description

1. Vacuum Chamber

A cross section[12] of the apparatus is shown in Fig. 4. Because of the large gas flow carrying the radioactivity from the cyclotron, the oven chamber was pumped by a 1400 liter/sec diffusion pump backed by a 100 liter/sec booster pump. Typical operating pressures were roughly 10^{-4} mm Hg in the oven chamber, 10^{-5} mm in the buffer chamber, and 10^{-6} mm in the main chamber. In the final apparatus (as shown in Fig. 4) there was a separately pumped detector chamber with a collimated entrance hole. This reduced the background and was an essential part of the experiment.

2. Magnets

A cross section of the three magnets is shown in Fig. 5.

(a) The six-pole permanent A magnet used has been previously described.[13] Repeated measurements with a Hall probe fluxmeter showed that the field strength was constant in time, with a maximum value (at the pole tips) of approximately 8000 G. The magnet length was 10.8 cm, and the radius of the axial hole was 0.16 cm.

(b) The B magnet was a permanent magnet with pole pieces made of Alnico V with pole tips and yoke structure made of Armco magnetic ingot iron. In a cylindrically symmetric quadrupole field the equipotentials are rectangular hyperbolas, $(x^2 - y^2) = \text{constant}$, and the resulting field gradient, $\nabla|\mathbf{H}| = C\hat{r}$, where r is the radial distance from the symmetry axis of the field and $\hat{r}$ is a unit vector in this direction. The pole tips were shaped using circular cutters to approximate closely equipotentials of the quadrupole field, both chosen to lie in the same quadrant of the quadrupole field and far enough from the symmetry axis of the field so that the gradient, $\nabla|\mathbf{H}|$, is approximately constant in both direction and magnitude over the full height of the beam entering the B magnet. Thus the field gradient is approximately

$$\nabla|\mathbf{H}| = [(H_{\max} - H_{\min})/l_g]\hat{\imath},$$

where $H_{\max}$ and $H_{\min}$ are the field strengths at the two pole tips, l_g is the gap width, and $\hat{\imath}$ is a unit vector along

[12] A detailed description of the design and operation of the apparatus is given by Martin Posner, thesis, Princeton University Technical Report NYO-2966 (unpublished), and Joseph L. Snider, thesis, Princeton University Technical Report NYO-2965 (unpublished).

[13] R. L. Christensen and D. R. Hamilton, Rev. Sci. Instr. 30, 356 (1959).

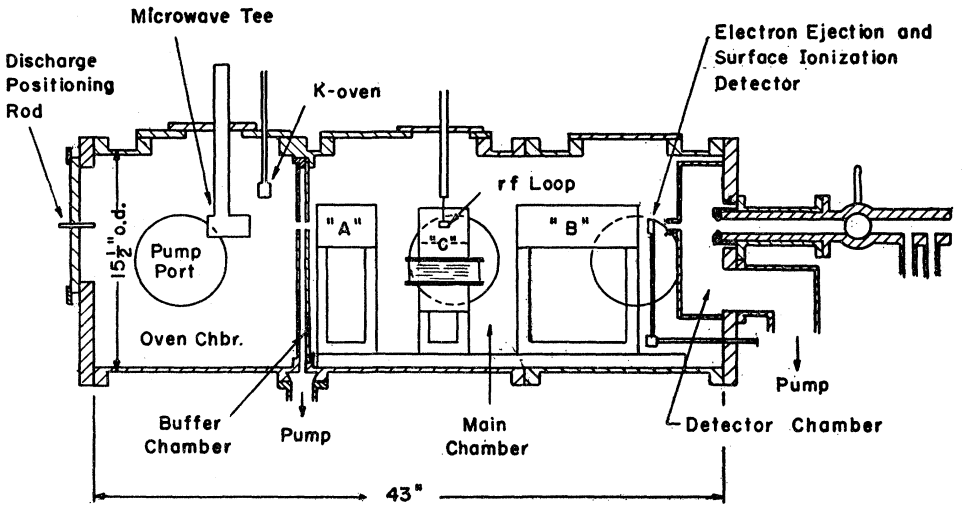

FIG. 4. Vertical cross section of the apparatus.

the horizontal symmetry axis of the pole tips (see Fig. 5).

The magnet was designed so that atoms having the most probable velocity from a source at a temperature of the order of 1000°K, having $g_J m_J = 1 (\gamma \sim 2.25 \times 10^{-8}$ $G^{-1})$, and entering the magnet in a direction parallel to its axis would be deflected through one-half the gap width. This insured complete separation of flopped from unflopped atoms, assuming the conditions to be fulfilled. The dimensions were: magnet length, 21.6 cm; gap width, 0.30 cm; entrance aperture, a square hole 0.15 cm on a side, on the weak-field side. The field strengths at the pole tips were: approximately 10 000 and 2000 G.

The "quadrupole" field was used instead of the conventional "two-wire" field because calculation showed that for flop-in operation, the deflection obtainable was significantly larger in the former case, assuming both magnets to have the same average field gradient. The calculation assumed that atoms entered the magnet parallel to the beam axis and had a representative value of the parameter γ. In the two-wire field the deflection depends strongly on where an atom enters, since the field gradient varies over the gap, and in flop-in operation using a six-pole A magnet the beam must enter the B magnet in a region of the two-wire field where the gradient, $\nabla|\mathbf{H}|$, is relatively weak. However, in the quadrupole field case, the gradient is essentially uniform across the whole gap. Since the beam entering the B magnet is relatively broad in this machine (due to the use of a six-pole A magnet), its average deflection would be smaller in the two-wire case and it would be smeared out as well. For a nonfocusing apparatus (i.e., use of a two-pole A magnet) with a narrow beam, the beam can be confined to a region of the "two-wire" field in which the gradient is essentially constant, and the "quadrupole" field no longer enjoys an advantage in deflection.

(c) The C magnet was an electromagnet constructed of Armco magnetic ingot iron with hypernom pole pieces separated from the yoke with quartz spacers. These nonmagnetic spacers serve to smooth the field and give increased homogeneity in the gap. This design follows that of Goodman.[14] The dimensions were: gap width, $\frac{1}{2}$ in.; length, $3\frac{1}{2}$ in.; pole-piece height, $2\frac{1}{2}$ in.

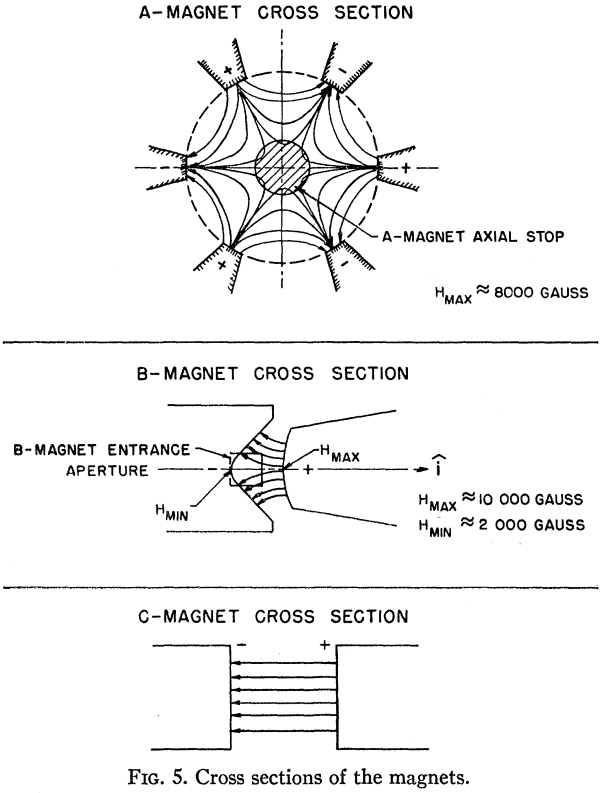

FIG. 5. Cross sections of the magnets.

[14] L. S. Goodman, Rev. Sci. Instr. 31, 1351 (1960). We would like to thank Dr. Goodman for informing us of his magnet design before publication and generously supplying us with the pole pieces.

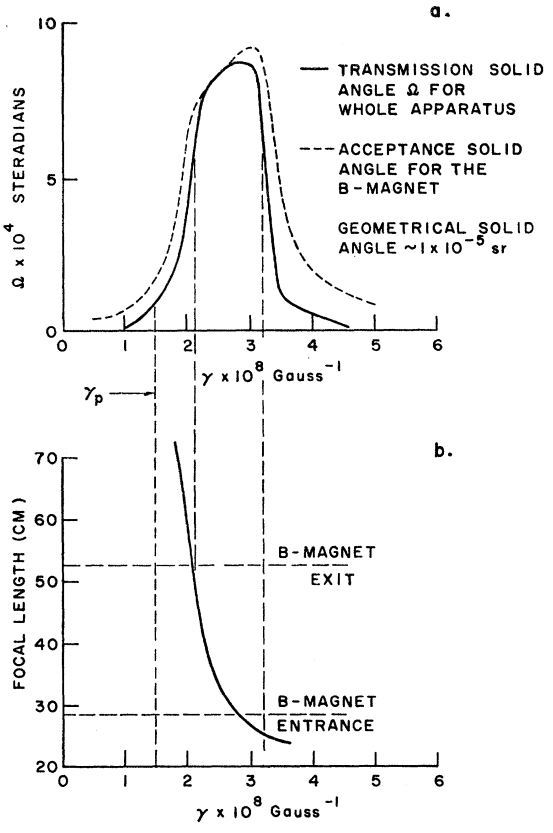

FIG. 6. (a) Transmission solid angle Ω versus the focusing parameter γ. (b) Focal length of A magnet (measured from the source position) versus γ. γ_p is the value of γ for which the atoms emerge from the A magnet parallel to the beam axis.

3. *Transmission Solid Angle*

The focusing and transmission properties of the completed apparatus are conveniently described by a transmission solid angle Ω, defined to be the total solid angle within which atoms can leave the source and reach the resonance detector, having undergone a transition in the C-field region. As pointed out before, the atomic trajectories in the apparatus are completely determined by the parameter γ. The transmission solid angle has been calculated as a function of γ assuming a point source and using the parameters of the completed apparatus. Each atom was assumed to undergo a transition from m_J to $-m_J$ in the C-field region, so that $|\gamma|$ is assumed to be the same in both magnets. The transmission solid angle, Ω, is plotted versus γ in Fig. 6(a) as the solid curve. The dashed curve is the solid angle within which atoms can leave the source and enter the B magnet. The similarity of the two curves indicates that the B magnet transmits nearly all of the atoms which enter it.

It is a property of the six-pole magnetic field [derivable from Eq. (7)] that all focused atom trajectories diverging from a point source and corresponding to a specific value of γ converge to a point focus on the symmetry axis of the magnet (within the range of angles accepted and passed by the magnet). In Fig. 6(b) this source-to-focal-point distance for the apparatus is plotted as a function of γ. This focal length depends only on the A magnet and the atomic species in question (through γ) and on the source position; it does not depend on the properties of the B magnet. It can be seen from Fig. 6 that the peak of the solid-angle curve occurs for foci which lie in the B magnet. The point marked γ_p is that value of γ for which all atoms emerging from a point source would emerge from the A magnet parallel to the axis. For $\gamma<\gamma_p$ the atoms are still diverging at the A magnet exit and no real focus exists.

The peak solid angle, $\Omega_{\max}=8\times10^{-4}$ sr, compares favorably with that for a focusing machine using two six-pole magnets. For a source temperature of 1000°K and $g_J m_J=1$ in the A magnet, averaging the solid angle over the beam velocity distribution gives

$$\bar{\Omega}\cong 2\times10^{-4}\text{ sr}.$$

Since one-half the atoms are rejected by the six-pole A magnet, this reduces $\bar{\Omega}$ to about 10^{-4} sr. The geometrical solid angle subtended by the detector at the source is $\cong10^{-5}$ sr, so the final result is that the effective transmission solid angle of the machine is about 10 times the geometrical solid angle.

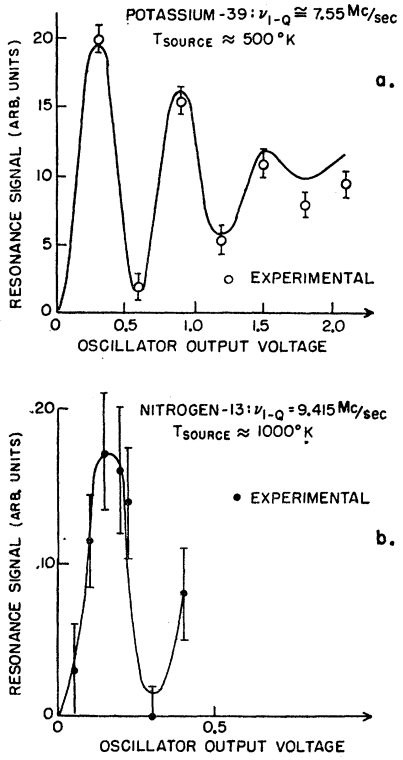

FIG. 7. K^{39} and N^{13} resonance signals versus oscillator output voltage ($\propto H_{rf}$). The solid curve drawn through the K^{39} experimental points (Part a) was calculated theoretically, as described in the text (Sec. III.B.3). The solid curve drawn through the N^{13} experimental points (Part b) is a visual fit to the data.

A general conclusion from the solid-angle curves is that the apparatus acts as a strong velocity selector. This fact was experimentally observed by measuring the rf-field dependence of the signal of a 1-quantum transition in K^{39}. Figure 7(a) shows the experimental points and a theoretical fit using the usual two-level resonance formula[7] averaged over a simplified velocity distribution of the form $N(v)=v^{-2}$ for $v_{\min}\leqslant v\leqslant v_{\max}$ and zero otherwise. The velocity spread used for the theoretical curve shown was approximately 5.5 to 7.7×10^4 cm/sec, which is in reasonable agreement with the range of velocities expected on the basis of the solid-angle calculation.

IV. N^{13} MEASUREMENTS

A. Production, Detection, and Resonance Techniques for N^{13} and Calibrating Beams

1. Production Techniques

a. N^{13}. The production system evolved from one previously used at Princeton for the study of C^{10} and O^{14} (Ref. 15). The target was in the form of a tightly packed powder enclosed in a thin foil through which the beam entered (18-MeV protons, typical beam current 0.4 μA). The idea was to find a suitable powder so that the radioactivity would be produced in the form of a gaseous molecule which could diffuse or be flushed out of the target.

The radioactivity was flushed out of the target by a continuous flow of neon gas at an input pressure of about 1 atm, and then travelled roughly 400 ft through a polyethylene tube to the atomic-beam machine. In this way, the source of radioactivity was maintained quite constant for as long a run as desired once equilibrium had been established. The amount of radioactivity flushed out was not sensitive to the input pressure. The transit time through the flow system was roughly 10 min, comparable with the 10-min half-life of N^{13}.

A variety of different target materials was tried. Melamine ($C_3N_6H_6$) was the one finally chosen. The N^{13} activity was produced in the reaction $N^{14}(p,pn$, or $d)N^{13}$. There appeared to be some irreversible change in the target material during use, since a target once used and then not bombarded for a time could not be used to obtain activity again. C^{11} was produced by the $N^{14}(p,\alpha)C^{11}$ reaction. An ascarite trap in the flow system was used to absorb C^{11}-bearing molecules.

Since the activity reached the machine in the form of molecules (possibly N_2) it was necessary to dissociate them into N^{13} atoms. This was accomplished by means of a microwave discharge. The discharge arrangement was similar to the one developed at MIT[16] and has been previously described.[17] The gas flow from the cyclotron passed into a quartz discharge tube mounted on the beam axis, and a continuous microwave discharge was maintained in the neon flushing gas. The discharge normally operated at roughly 5 mm Hg pressure, and the flux of N^{13} atoms effusing from the orifice in the quartz discharge tube (typically 0.020–0.030 in. in diameter) under these pressure conditions was of the order of 10^7 atoms/sec.

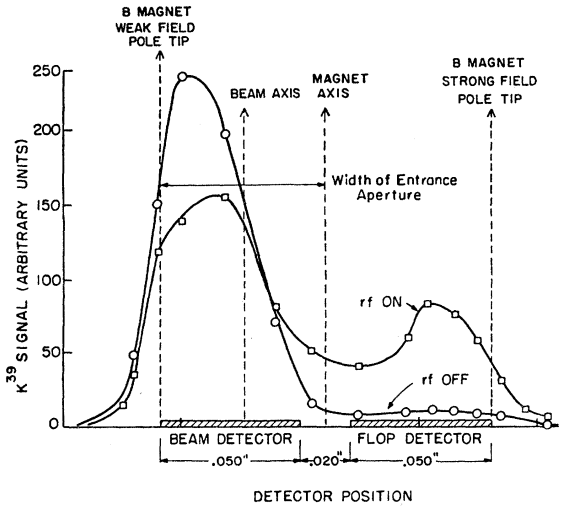

FIG. 8. K^{39} beam profile taken at B-magnet exit. The cross-hatched lines indicate the positions of the beam and flop detectors for the N^{13} experiment.

A comparison of the N^{13} radioactivity collected on activated-charcoal targets with discharge on and off indicated a fractional dissociation of the order of 0.1 to 0.4. (The collection efficiency of activated charcoal was greater for the N^{13} bearing molecules than for the nitrogen atoms.) Another qualitative indication of dissociation by the discharge was the fact that the count rate on the hot titanium N^{13} detectors dropped to close to background when the discharge was turned off. (The hot titanium detectors were relatively highly efficient in collecting nitrogen atoms as compared to their efficiency in collecting the N^{13}-bearing molecules. See following section.)

b. Argon. A microwave discharge in argon served as a source of metastable argon atoms with which the magnetic field was calibrated.

c. Potassium. The potassium beam was generated by a conventional resistance heated oven which could be lowered in front of the discharge assembly.

2. Detection Techniques

a. Argon and potassium. Beams of potassium and metastable argon were detected using a standard surface-ionization or electron-ejection detector.[7]

[15] R. Sherr, H. R. Muether, and M. G. White, Phys. Rev. **75**, 282 (1949).

[16] J. C. King and J. R. Zacharias, *Advances in Electronics and Electron Physics*, edited by L. Marton (Academic Press, Inc., New York, 1956), Vol. 8. p. 1.

[17] Robert L. Christensen, Technical Report NYO-8016, Princeton University (unpublished), and R. L. Christensen, D. R. Hamilton, H. C. Benewitz, J. B. Reynolds, and H. H. Stroke, Phys. Rev. **122**, 1302 (1961).

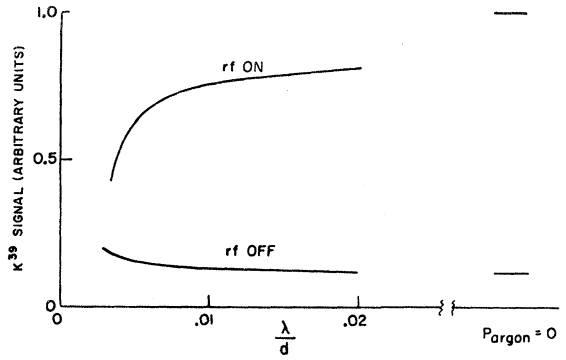

FIG. 9. K^{39} signal versus λ/d (mean free path over source diameter). λ was controlled by argon gas flowing through the potassium oven. $\lambda/d \simeq 0.02/p$, where p is the pressure of argon in mm Hg. It was calculated using the total argon-potassium cross sections listed by Ramsey (Ref. 7).

b. N^{13}. The nitrogen-13 detector consisted of two targets positioned behind the B-magnet exit, one of which served as the resonance detector (flop target) and the other as a beam monitor (beam target). (See Fig. 3.) The ratio of counts collected on the two targets (flop-to-beam or F/B ratio) is independent of absolute beam size and rises on resonance.

A beam profile of the K^{39} beam, obtained by moving the surface ionization detector across the beam at the B-magnet exit, is shown in Fig. 8. The general features of such profiles are determined by the dimensions, field strengths, and alignment of the deflecting magnets and the source alignment. A comparison of the profiles with and without a resonance gives useful information regarding the best position for a detector for radioactive isotopes. A good flop-in resonance signal can be obtained almost all the way across the strong-field half of the B-magnet gap as shown. The N^{13} detector was therefore designed with two vertical target strips, each covering approximately half the B-magnet gap, with a 0.020-in. separation between them as shown in Figs. 8 and 3.

Measurements were made of relative sticking coefficients for N^{13} atoms for a number of substances and are presented in Table II. It was hoped that N^{13} atoms would react chemically with surfaces at room temperature, but many surfaces proved bad even though care was taken to clean them. Heated metal foils finally proved successful, and titanium was used. The temperature of each of the two titanium detector foils could be controlled independently by varying the current through it and was kept at approximately 1025°C as checked with an optical pyrometer. In the temperature range 950–1100°C, the collection efficiency was independent of temperature. The fact that the collection efficiency of the heated foils increases with increasing oxidation potential strongly suggests that the sticking mechanism is chemical in nature and involves the oxidation of target atoms by nitrogen atoms.

TABLE II. List of target materials tried and their relative collection efficiency for nitrogen atoms. The oxidation potentials listed were taken from the 41st edition of the *Handbook of Physics and Chemistry* (Chemical Rubber Publishing Company, Cleveland, Ohio) and are measured relative to the hydrogen-hydrogen ion couple.

Material	Temperature	Relative collection efficiency	Oxidation potential (V)
Cu, Fe, Au, Hg, Ti, Nb, Ag, Sn	room	1	—
K	room	~10	+2.92
Fe	1025°C	~10	+0.44
Nb	1025°C	20–50	+1.1
Ti	1025°C	100–200	+1.63

The small sticking probability of N^{13} atoms on metals at room temperature means that these atoms bounce around many times before they stick to the walls or are pumped out of the vacuum chamber. This creates a large background on the resonance detector. The main experimental problem was the elimination of this background. Several of the methods tried, although they did not succeed, may perhaps be of some interest.

The general rule for producing collimated beams is that the mean free path λ should be approximately equal to or greater than the source diameter d (Knudsen condition).[7] In a microwave discharge the pressure must be high enough to sustain the discharge, and this results in $\lambda/d \approx 0.01$ for the discharge conditions used in this experiment. We therefore decided to investigate the applicability of the Knudsen condition. A potassium oven was constructed so that argon could also flow through the oven. The K^{39} signals on resonance and with no rf field were observed as a function of argon pressure, i.e., as a function of λ/d (λ was calculated using the *total* argon-potassium collision cross sections listed by Ramsey.[7]) The oven temperature, and hence the flow of potassium, was kept constant. The results are shown in Fig. 9. It can be seen that both the machine background and the resonance signals remain relatively insensitive to the source pressure for $\lambda > 0.005\ d$. For our operating pressure we conclude that this cannot be an important source of machine background.

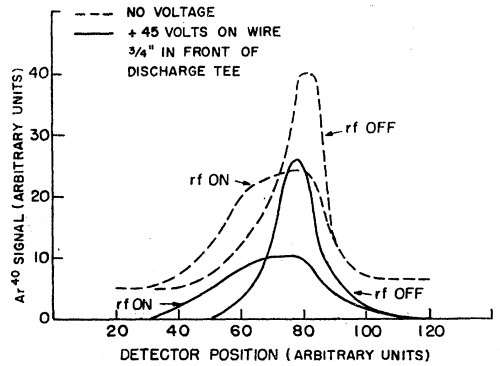

FIG. 10. Argon beam profiles taken with a positively biased wire next to the discharge tube orifice.

Another idea which was tried was to introduce a wire near the front end of the discharge tube and apply a positive voltage to it. (The application of negative voltages had no effect.) This collected electrons from the beam immediately after they left the discharge and had the effect of "local pumping." This had a significant effect on argon profiles at high pressures as can be seen in Fig. 10. Unfortunately, the effect on the N^{13} background was negligible.

The solution to the problem of high background was found to be the installation of a detector chamber. (See Figs. 3 and 4.) The titanium target foils were mounted on the end of a probe which was inserted through a vacuum lock into the separately pumped detector chamber, so that the foils were about 6 in. behind the B-magnet exit. This detector position presumably prevented unflopped atoms which scatter from the weak field pole tip of the B magnet from reaching the flop detector. (See Fig. 3.)

After exposure to the beam, typically for a 10-min period, the detector probe was removed from the machine and the target foils mounted on metal slugs with scotch tape. The slugs were then inserted into counters so that the foils were close to $\frac{1}{2}$-in.-diam, 1-mm-thick plastic scintillators. The decay positrons were counted using standard electronics with an integral baseline set by means of a Tl^{204} calibrating source. For a 10-min exposure and 10-min counting period, the "beam" foil typically registered 500 counts while the "flop" foil gave about 125 counts off resonance, rising to about 225 counts on resonance. Thus, the F/B ratio rose from about 0.25 off resonance to about 0.45 on resonance.

3. *Magnetic Resonance Techniques*

For observing $\Delta m_F = \pm 1$ (or π) transitions, a "solenoid" rf loop oriented parallel to the beam was used. This consisted of 12 turns of No. 14 wire with inner diameter $\frac{5}{16}$ in. and length $\frac{13}{16}$ in. which was soldered to a coaxial connector. It was driven in the frequency range 0.1–30 Mc/sec by a Rohde-Schwarz SMLR signal generator. At higher frequencies a Rohde-Schwarz SMLM was used. This type of loop has the advantage that at low frequencies (a few Mc/sec), for which its reactance is small compared with the internal impedance of the generator, it produces a larger oscillating magnetic field than a similar single-turn loop in direct proportion to the number of turns.

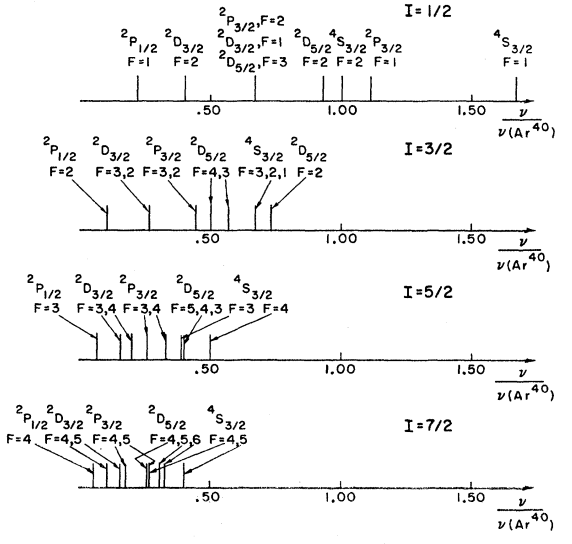

FIG. 11. Zeeman resonance frequencies for the atomic states of nitrogen and half integral nuclear spins in units of $\nu(Ar^{40})$.

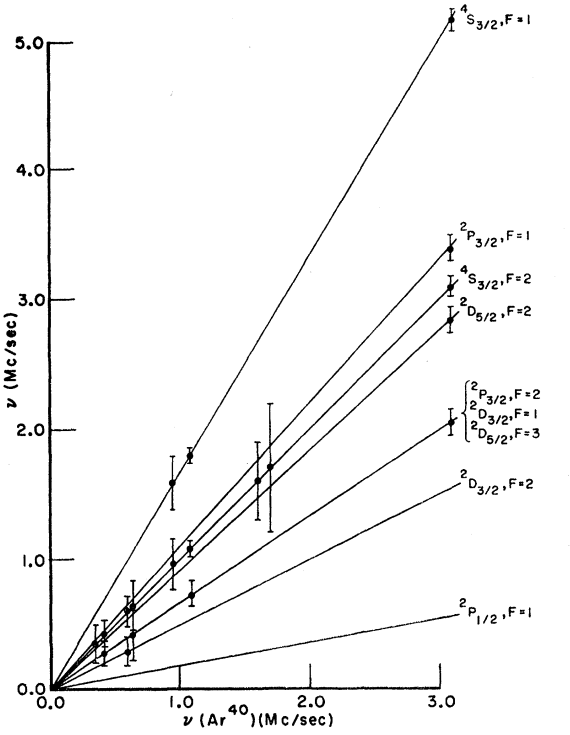

FIG. 12. Observed low-field resonances versus magnetic field in units of the Ar^{40} resonance frequency. The solid lines represent the expected frequencies for $I=\frac{1}{2}$. The error flags represent the linewidths of the resonances.

For observing direct $\Delta F=1$, $\Delta m_F=0$, transitions a strap loop made from a strip of copper was used. A hole for the beam was drilled through the strip, and two cylindrical shields helped to keep the return flux from the path of the beam. The line shape observed with this loop was interesting and is discussed below.

B. Data and Moment

The atomic valence electrons of nitrogen are in a p^3 configuration which gives rise to the multiplets: $^4S_{3/2}$(ground state), ^2D(2.38 eV), and ^2P(3.57 eV).[18] The ^2D and ^2P doublets are metastable and were populated in the microwave discharge. Although resonances were

[18] E. U. Condon and G. H. Shortley, *The Theory of Atomic Spectra* (Cambridge University Press, London, 1953), and C. E. Moore, *Atomic Energy Levels*, Natl. Bur. Std. Circ. 467 (1949).

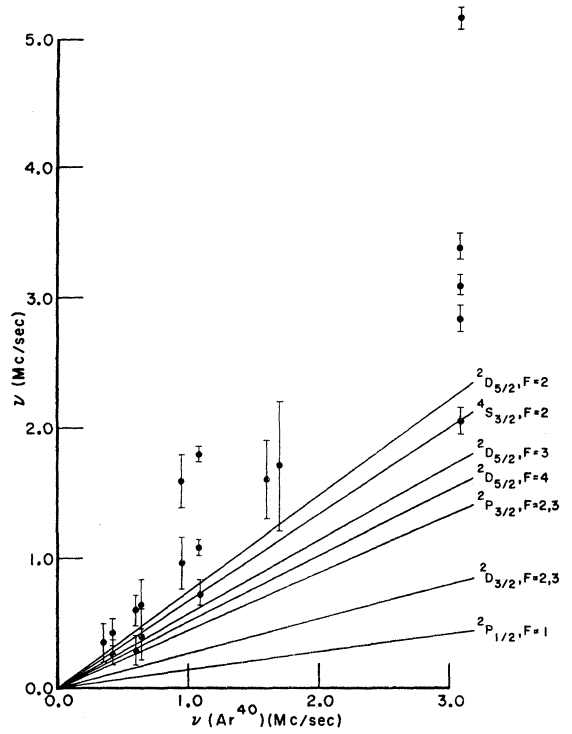

FIG. 13. Same data as in Fig. 12 but the theoretical lines are for $I=\frac{3}{2}$.

observed in these doublets the hyperfine structure measurements were made in the $^4S_{3/2}$ ground state. It can be shown that in S states the hyperfine structure interaction is a contact interaction.[19] However, since p electrons have no contact interaction, the hyperfine structure of the $^4S_{3/2}$ state of nitrogen is due to the contact interaction which results from the exchange polarization of the s orbitals.[20]

1. Spin

The possible presence of the metastable states makes the number of possible resonances quite large. Figure 11 gives the possible Zeeman resonance frequencies observable with the machine optics for each nuclear spin up to $I=\frac{7}{2}$ in terms of $\nu(\mathrm{Ar}^{40})$. Nuclear spin-$\frac{1}{2}$ has the highest Zeeman frequencies. Resonances were observed in several magnetic fields up to approximately 1.5 G. In Fig. 12 the data are presented along with the predicted positions for $I=\frac{1}{2}$. The data are seen to be consistent with $I=\frac{1}{2}$. In particular, from the data at the highest field it is quite clear that the resonances in the metastable states are being observed. In Fig. 13 the same data are plotted with the predictions for $I=\frac{3}{2}$. It can be seen that the assumption of $I=\frac{3}{2}$ does not fit the data. Therefore, we conclude that $I=\frac{1}{2}$,[21] which is the result expected since N^{13} should have the same spin as C^{13}. Subsequent measurement of the hyperfine structure splitting $\Delta\nu$ confirmed the spin assignment (see following section).

2. Hyperfine Structure Measurements: Magnetic Moment

A preliminary value of the hyperfine structure splitting, $\Delta\nu$, in the $^4S_{3/2}$ state was obtained by following the $F=2$, $m_F=1$ to $F=2$, $m_F=0$ transition (the one labeled α in Fig. 2) out of the Zeeman region to a magnetic field of approximately 12 G. In Fig. 14 two of the resonance curves are shown. The linewidth is approximately 70 kc/sec and is mostly due to the transit time through the loop. A power dependence of one of the resonances is shown in Fig. 7 and compared to the power dependence of a one quantum transition in K^{39}. By comparison of the relative radio-frequency power needed for maximum signal for the K^{39} and N^{13} resonances shown in Fig. 7 it was concluded that the N^{13} resonance was also a one quantum transition (the analysis was based on theoretical calculations by Hack[22] of optimum radio-frequency power for multiple-quantum transitions). From the resonance frequencies observed at three fields it was determined that $\Delta\nu=33.2\pm0.3$ Mc/sec.[23]

In order to improve the accuracy, the transition $F=1$, $m_F=0$ to $F=2$, $m_F=0$ (the one labeled β in Fig. 2) was observed at small magnetic fields. The frequency of this transition was given in Sec. II. Note that the transition is field insensitive: Its frequency differs from $\Delta\nu$ only by second and higher order terms in H_0. This fact provided the principal means of identifying this transition. In the $\Delta F=0$ transition $\Delta m_F=1$, and therefore, a π loop was used, which has the oscillating magnetic field normal to the direction of the C field (as noted in Part A.3 of this section). For the $\Delta F=1$ transition we have a σ transition, and therefore the oscillating magnetic field must be parallel to the C-field

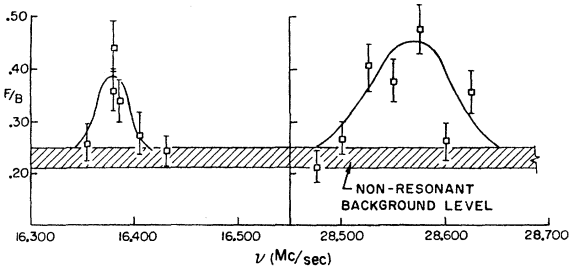

FIG. 14. $\Delta F=0$, N^{13} resonances which were used to obtain a preliminary value of the hyperfine structure splitting. The nonresonant background F/B level was checked periodically by making exposures with the rf power off.

[19] E. Fermi and E. Segrè, Z. Physik **82**, 729 (1933).
[20] N. Bessis, H. Lefebvre-Brion, and C. M. Moser, Phys. Rev. **124**, 1124 (1961).
[21] J. L. Snider, M. Posner, A. M. Bernstein, and D. R. Hamilton, Bull. Am. Phys. Soc. **6**, 224 (1961).
[22] M. N. Hack, Phys. Rev. **104**, 84 (1956).
[23] M. Posner, J. L. Snider, A. M. Bernstein, and D. R. Hamilton, Phys. Rev. Letters **7**, 173 (1961).

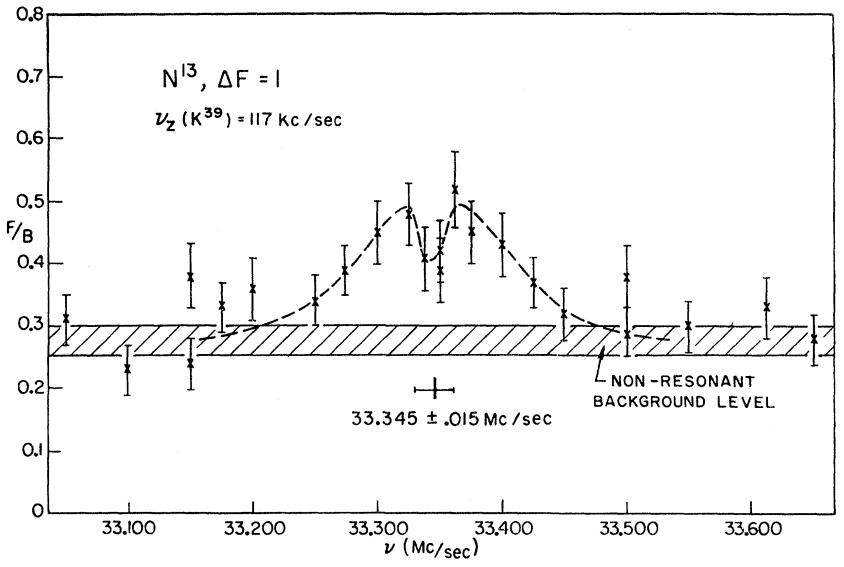

FIG. 15. $\Delta F=1$ resonance in N^{13}. Note the dip at the center of the resonance. (See text and Ref. 24.)

direction. In loops of this type it is known that the line shapes can have minima at the resonance frequency.[24] In order to reduce this effect but not to eliminate it completely, a shielded loop was used. One of the resonances obtained with this loop is shown in Fig. 15.

The results obtained are presented in Table III. The magnetic field is given in terms of the K^{39}, $\Delta F=0$, Zeeman resonance frequency with which it was calibrated [see Eq. (5), Sec. II]. The average value for $\Delta\nu$ is (33.347±0.020) Mc/sec.[25] Then $|a|=16.673$ ±0.010 Mc/sec.

Precision measurements of μ_I and a have been made for N^{14} and N^{15} (Ref. 26). We therefore use the Fermi-Segrè formula to deduce the moment of N^{13}. From μ_I and a for N^{14}, neglecting the diamagnetic correction

$$|\mu_I(N^{13})|_{\text{uncorr}}=0.32186\pm0.00019 \text{ nm}.$$

From μ_I and a for N^{15},

$$|\mu_I(N^{13})|_{\text{uncorr}}=0.32218\pm0.00019 \text{ nm}.$$

The $N^{14}-N^{15}$ hyperfine structure anomaly of 0.1%[26] accounts for the difference between these two values of $\mu_I(N^{13})$. It is not clear which of the values is more trustworthy; we take the mean value and increase the error to include the possible effect of hyperfine structure anomalies. Then

$$|\mu_I(N^{13})|_{\text{uncorr}}=0.32202\pm0.00035 \text{ nm}.$$

Applying the diamagnetic correction[27] to the above value gives

$$\mu_I(N^{13})=-0.32212\pm0.00035 \text{ nm}.$$

Although we have given the sign as negative, we have only measured its absolute magnitude and inferred that its sign must be negative as in the case of N^{15}.

TABLE III. Summary of the N^{13} $\Delta\nu$ measurements, made by observation of the field insensitive σ transition ($F=2, m_F=0$) → ($F=1, m_F=0$). The magnetic field is given in terms of the K^{39} Zeeman frequency, $\nu_Z(K^{39})$ [see Eq. (5), Sec. II].

All frequencies in Mc/sec		
$\nu_Z(K^{39})$	$\nu(N^{13})$	$\Delta\nu$
0.075±0.007	33.343±0.025	33.342±0.026
0.081±0.010	33.355±0.020	33.353±0.021
0.117±0.010	33.345±0.015	33.342±0.016
0.240±0.020	33.375±0.037	33.361±0.038
	Weighted mean[a]:	33.347±0.020

[a] The individual values of $\Delta\nu$ have been weighted according to the inverse squares of their uncertainties.

V. INTERPRETATION

The results of the present measurement along with those mirror nuclei whose moments have been recently measured are given in Table IV.

The numbers presented in Table IV provide partial support for the belief that under ideal circumstances the sum of magnetic moments of a pair of mirror nuclei is equal to the sum of Schmidt moments for that pair. We expect this to be true if the nucleus is in a single-particle state and if the mesonic current contributions are equal and opposite in mirror nuclei. The assumption of a pure single-particle $s_{1/2}$ ground state for the mass-19

[24] G. K. Woodgate and R. W. Hellwarth, Proc. Phys. Soc. (London) **A69**, 588 (1956).
[25] R. A. Haberstroh and D. R. Hamilton, Bull. Am. Phys. Soc. **7**, 25 (1962).
[26] L. W. Anderson, F. M. Pipkin, and J. C. Baird, Phys. Rev. **116**, 87 (1959) and W. W. Holloway, Jr., E. Lüscher, and R. Novick, Phys. Rev. **126**, 2109 (1962).
[27] This diamagnetic correction was made using the results of W. C. Dickinson, Phys. Rev. **80**, 263 (1950).

TABLE IV. Magnetic moments of mirror pairs of nuclei. μ_{exp} is the experimental moment and $\mu_{Schmidt}$ the single-particle moment. All values of μ_{exp} except those for which a footnote is given, are taken from D. Strominger, J. M. Hollander, and G. T. Seaborg, Rev. Mod. Phys. **30**, 585 (1958). All moments listed are in units of nuclear magnetons.

Nucleus	μ_{exp}	$\mu_{Schmidt}$	$(\mu_{exp}-\mu_{Schmidt})$
He^3	−2.127	−1.913[d]	−0.214
H^3	2.979	2.793[d]	0.186
Sum	0.852	0.880	−0.028
C^{13}	0.702	0.638[e]	0.064
N^{13}	−0.322[a]	−0.264[e]	−0.058
Sum	0.380	0.374	0.006
O^{15}	0.719[b]	0.638	0.081
N^{15}	−0.283	−0.264	−0.019
Sum	0.436	0.374	0.062
F^{19}	2.627	2.793[d]	−0.166
Ne^{19}	−1.886[c]	−1.913[d]	0.027
Sum	0.741	0.880	−0.139

[a] This paper.
[b] E. D. Commins and H. R. Feldman, Phys. Rev. **131**, 700 (1963).
[c] E. D. Commins and D. A. Dobson, Phys. Rev. Letters **10**, 347 (1963).
[d] For an $(s_{1/2})$ single-particle state.
[e] For a $(p_{1/2})$ single-particle state.

isobars is known to be incorrect,[28] and it is not surprising that this pair of mirror nuclei shows the maximum deviation. As discussed in more detail below, the mass-13 wave functions are believed to be intermediate between L-S and j-j coupling.[28–32] Only the mass-15 wave function would qualify as single-particle wave functions in the shell model. It therefore seems surprising that the sum of the deviations from the Schmidt moments is larger for the mass-15 moments than for the mass-13 moments. However, since this discrepancy amounts to only 0.06 nm it is probably beyond the accuracy of present theory.

It would be desirable to analyze N^{13} and C^{13} as Sachs did He^3 and H^3. For this purpose one cannot use the magnetic moment of each isotope as one is trying to determine an unknown part of the magnetic moment operator. Therefore, one uses only the sum of the magnetic moments of a pair of mirror nuclei since the sum should be independent of meson exchange effects if contributions to the magnetic moment operator obey the Sachs mirror theorem.[3]

The mass-13 wave functions have already been worked out as a function of the degree of intermediate coupling as specified by a parameter y, so for $y=0$ there is pure L-S coupling, for $y=1$ there is pure j-j coupling, and for intermediate y there is intermediate coupling.[29,31] One might therefore hope to determine y from the sum of the magnetic moments. This calculation has been performed by Kurath,[30] who finds that the sum of the magnetic moments of N^{13} and C^{13} should lie between 0.365 and 0.376 nm over the entire range of y. However, in view of the insensitivity of the calculated sum to y, the experimental sum does not accurately tell us the value of y which characterizes the wave functions. Thus, the comparison of the experimental sum with the sum calculated for the intermediate coupling model does not allow us to make a clear-cut prediction of the individual moments which would lead to a determination of the meson exchange contributions.

An argument that can be raised against the calculation of magnetic moments on the basis of the intermediate coupling model is that the calculation was not done in a consistent manner. Since the Hamiltonian used included effects of exchange- and velocity-dependent forces, care must be exercised regarding the choice of the current operator. The choice of the current operator is restricted by the quantum-mechanical form of the equation of continuity for the current and charge density operators, j and ρ:

$$\operatorname{div}\mathbf{j}+(i/\hbar)[\mathfrak{H},\rho]=0.$$

The employment of the normal quantum-mechanical formula for $\mathbf{j}$ violates the continuity equation if exchange forces are present in the Hamiltonian $\mathfrak{H}$, and additions to $\mathbf{j}$ usually referred to as "exchange current" contributions are then required. The actual calculations did not take these additions into account and therefore may not be considered as self-consistent.

The actual interaction is probably an effect of meson exchange, which is not exactly describable by ordinary phenomenological potentials. Since complete treatments of this question are still unavailable, it appears reasonable at present to treat the problem by means of the phenomenological Hamiltonian and to hope, that through comparison with experiment, questions of limits of validity of the Hamiltonian and of the magnitude of exchange current effects will be at least partly clarified.

One might ask whether the fact that the N^{13} and C^{13} moments both lie outside the Schmidt moments by equal and opposite amounts demonstrates the existence of mesonic current effects. In Fig. 16 the calculated magnetic moments of N^{13} and C^{13} are plotted as a function of y (constructed from Ref. 31); if the coupling were pure j-j, the fact that the moments lie outside the Schmidt lines would indicate the existence of meson exchange effects. However, it is seen that for sufficiently small y the predictions lie outside the Schmidt limits. In fact for the generally accepted value of $y\approx\frac{1}{2}$ we get reasonable agreement between theory and experiment.

However, we believe that this agreement cannot be taken as evidence that the intermediate coupling wave functions with the ordinary magnetic moment operator fit the data so well that mesonic current effects are ex-

[28] For a discussion of the ground state of the mass-19 isobars, see p. 350 of the review article on the intermediate coupling shell model by J. P. Elliot and A. M. Lane, *Handbuch der Physik*, edited by S. Flügge (Springer-Verlag, Berlin, 1957), Vol. 39, p. 241.
[29] The $A=13$ wave function in intermediate coupling is given in detail by M. H. Macfarlane and J. B. French, Rev. Mod. Phys. **32**, 567 (1960).
[30] D. Kurath, Phys. Rev. **124**, 552 (1961).
[31] A. M. Lane, Proc. Phys. Soc. (London) **A66**, 977 (1953).
[32] A. M. Lane, Rev. Mod. Phys. **32**, 519 (1960).

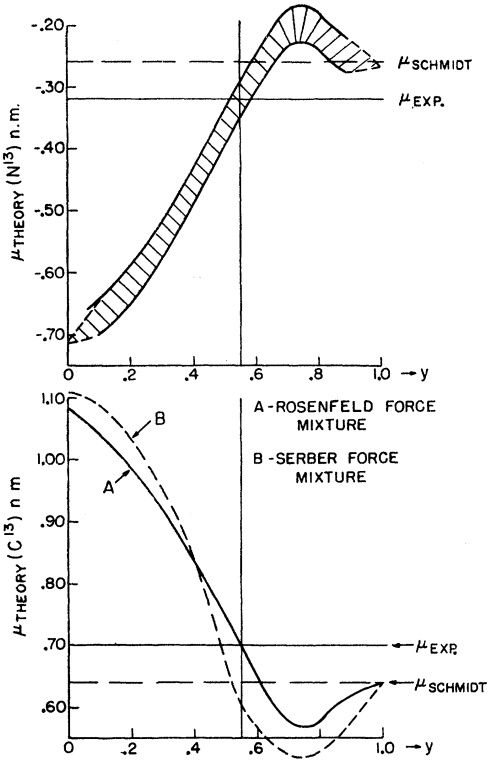

FIG. 16. The theoretical prediction of the intermediate coupling shell model for the magnetic moments μ for the $A=13$ isobars versus the intermediate coupling parameter y. The graph for N^{13} was constructed from the relation $\mu(C^{13})+\mu(N^{13})=0.37\pm0.04$ nm and results listed in Ref. 31.

cluded. In the first place, the belief that $y\approx\frac{1}{2}$ comes from the fit of the C^{13} magnetic moment, the beta decay ft value, the $M1$ transitions from the $\frac{3}{2}$ state to the $\frac{1}{2}$ ground state, and from experiments yielding reduced widths. (See Refs. 29, 32, and 33.) Because of the uncertainty in the magnetic moment operator, and a similar uncertainty in the axial vector beta decay matrix element, the results of the first three experiments do not unambiguously determine y. As to reduced widths, these are extracted from experiments by a nuclear reaction theory, and one does not expect the accuracy to be any greater than about 20%. In the second place, the uncertainties in the ratio of the direct-to-exchange integral (L/K) and in the force mixture used for the residual interaction in the Hamiltonian directly affect the calculated wave function, and therefore may indirectly result in errors in the calculated magnetic moments comparable in size to any mesonic current effects present.

Therefore, although it is possible in principle that the magnetic moments of C^{13} and N^{13} could be explained by the intermediate coupling shell model, we will probably never know, unless y, the force mixture, and the ratio of direct to exchange integral can be predicted from first principles.

The fact that all of the moments of the mass 3, 13, and 15 pairs lie outside of the Schmidt moments seems to be the best indication that mesonic-current contributions to nuclear magnetic moments do exist.

ACKNOWLEDGMENTS

The authors are indebted to Professor G. Breit for his careful reading of the introduction and interpretation sections of the article. The authors also wish to thank both Professor Breit and Professor F. Villars for some enlightening and helpful discussions about meson-exchange currents.

[33] W. E. Burcham, *Handbuch der Physik*, edited by S. Flügge (Springer-Verlag, Berlin, 1957), Vol. 40, p. 1.